PREPRINT 431

SEPTEMBER 2015

RWTH

igpm

Numerical Discretization of Coupling Conditions by High-Order Schemes

Mapundi K. Banda, Axel-Stefan Häck and Michael Herty

Institut für
Geometrie und Praktische Mathematik
Templergraben 55, 52062 Aachen, Germany

Date: September 8, 2015.
University of Pretoria, Pretoria, South Africa mapundi.banda@up.ac.za .
RWTH Aachen University, Aachen, Germany; haeck@igpm.rwth-aachen.de.
RWTH Aachen University, Aachen, Germany; herty@igpm.rwth-aachen.de.

NUMERICAL DISCRETIZATION OF COUPLING CONDITIONS BY HIGH-ORDER SCHEMES

MAPUNDI K. BANDA, AXEL-STEFAN HÄCK, AND MICHAEL HERTY

Abstract. We consider numerical schemes for 2×2 hyperbolic conservation laws on networks coupled by possibly nonlinear coupling conditions at nodes of a network. We develop high-order finite volume discretizations including coupling conditions. The reconstruction of the fluxes at the node is obtained using derivatives of the parameterized algebraic conditions imposed at the nodal points in the network. Numerical results illustrate the expected theoretical behavior.

35R02, 35Q35, 35F30

Keywords. numerical methods, higher-order coupling, networks of fluid dynamics,

1. Introduction

We are interested in the high order numerical discretization of flow problems on networks where the dynamics are governed by 2×2 systems of nonlinear hyperbolic partial differential equations. Among the many examples where such systems arise are traffic flow [22, 23, 27, 29], production networks [19, 21, 28], telecommunication networks [20], gas flow in pipe networks [2, 9–11, 13, 14] or water flow in canals [3, 4, 26, 33]. Mathematically, flow problems on networks are boundary value problems where the boundary value is implicitly defined by a coupling condition. This condition is either physically or mathematically motivated and may consist of algebraic conditions coupling the flow in different arcs or may consist of ordinary differential equations. We are interested in finite–volume methods to resolve the hyperbolic dynamics. Most of the available finite volume methods solve the coupling condition explicitly [1, 6–8]. For the evolving state at the node, a Godunov–type scheme [1] or kinetic scheme [6] is applied to determine the fluxes at the cell interface. Those schemes are explicit in time and therefore the dynamics on different arcs decouple contrary to an implicit discretization (in time) [31].

We develop a second–order finite volume scheme for general 2×2 hyperbolic systems on networks. The crucial point is the derivation of a suitable numerical flux at the nodal point where we apply high order reconstruction using temporal derivatives of the state at the node. We use a characteristic decomposition of the temporal derivative of the solution at the nodal point and estimate the outgoing information using spatial derivatives. This procedure has been applied to (pure) boundary value problems in the context of finite volumes for example in [37–39] and mimics the Cauchy–Kowalewski theorem for sufficiently smooth solutions. We show that the derived scheme coincides

Date: September 8, 2015.

University of Pretoria, Pretoria, South Africa mapundi.banda@up.ac.za .
RWTH Aachen University, Aachen, Germany; haeck@igpm.rwth-aachen.de.
RWTH Aachen University, Aachen, Germany; herty@igpm.rwth-aachen.de.

with a second–order discretization in the case of two connected arcs, we validate the discretization by reformulating a classical boundary value problem using coupling conditions and we present numerical results for gas flow in pipe networks. The only other approach to high order coupling conditions on networks which we are aware of is [5]. Therein, additional ghost cells for each connected arc are introduced to recover a solution and the information on the temporal derivatives is obtained without characteristic decomposition. We discuss the relation between the schemes in Section 3.

2. Motivation and numerical scheme

As in [1, 2, 13, 14] we consider the following model for flows on graphs. This situation covers examples in gas pipe networks, traffic flow and water flow in open canals. We consider a single vertex connected to n arcs $j = 1, \dots, n$. The arcs extend to infinity hence they are parameterized by the interval $[0, \infty)$. The vertex is located at $x = 0$ for all arcs.

For simplicity of the presentation, we assume that the flux f is the same on all connected arcs. Let $f \in C^4(\mathbb{R}^2; \mathbb{R}^2)$ and $u_j(x,t) : \mathbb{R}_0^+ \times \mathbb{R}_0^+ \to \mathbb{R}^2$ for $j = 1, \dots, n$ where u_j denotes the conserved variables on arc j. The dynamics of u_j are governed by

$$\partial_t u_j + \partial_x f(u_j) = 0, \ t \geq 0, \ x \geq 0, \tag{1}$$

$$u_j(x, 0) = u_{j,0}(x), \ x \geq 0, \tag{2}$$

$$\Psi(u_1(0+, t), \dots, u_n(0+, t)) = 0, \ t \geq 0 \tag{3}$$

where $\Psi : \mathbb{R}^{2n} \to \mathbb{R}^n$ is the possibly nonlinear coupling condition.

We assume that Ψ fulfills a transversality condition (4) below:

$$\det \ [D_1\Psi(\hat{u}) r_2(\hat{u}_1), \dots, D_n\Psi(\hat{u}) r_2(\hat{u}_n)] \neq 0. \tag{4}$$

which ensures well–posedness of problem (1) to (3). Here, $D_j\Psi(\hat{u}) = \frac{\partial}{\partial u_j}\Psi(\hat{u})$ and $\hat{u} \in \mathbb{R}^{2n}$ is a steady state solution to (1) such that $\Psi(\hat{u}) = 0$. We refer to [14, Definition 3.1] and [14, Theorem 3.2] for more details on the definition of the solution and assumption on the characteristic fields as well as the existence and uniqueness result.

Furthermore, the Jacobian of f, $Df(\hat{u}_j)$, admits a strictly negative $\lambda^1(\hat{u}_j)$ and strictly positive eigenvalue $\lambda^2(\hat{u}_j)$ with linearly independent (right) eigenvectors r_1 and r_2, respectively. The associated characteristic fields are assumed to be either genuine nonlinear or linearly degenerate.

Now we present the finite volume method [32, 34] which is employed to numerically solve (1)-(3). This is essentially based on the proof of the well–posedness.

Consider a regular (uniform) grid of cell size $\Delta x = x_{i+1} - x_i$, where x_i, x_{i+1} are the cell centers and time step $\Delta t = t^{m+1} - t^m$, chosen so that the CFL condition [17] $\lambda_{\max}\Delta t \leq \Delta x$, where $\lambda_{\max}$ is the largest wave speed, is satisfied. We assume the grid-points are labeled by $i, m \in \mathbb{N}_0$ such that $x_0 = \frac{\Delta x}{2}$ and $t^0 = 0$. Hence, the center of the first cell $i = 0$ in each arc is located at x_0 and the physical node is located at the boundary $x = 0$. For some compact domain $\Omega \subset \mathbb{R}^2$ such that $u_{j,0} \in \Omega$ and $u_j(x,t) \in \Omega$, we compute the spectral radius ρ of Df as

$$\lambda_{\max} = \max_{v \in \Omega} |\rho(Df(v))|. \tag{5}$$

In addition the cell boundaries (interfaces) are denoted $x_{i-1/2}$, on the left, and $x_{i+1/2}$ on the right such that $\Delta x = x_{i+1/2} - x_{i-1/2}$. Sometimes the notation $\mathcal{I}_i := [x_{i-1/2}, x_{i+1/2}]$ will be used. The discretization is undertaken component-wise for each u_j. Hence the cell average of u_j in cell i at time t^m is denoted by $U^m_{j,i}$ and defined as

$$U^m_{j,i} := \frac{1}{\Delta x}\int_{x_{i-\frac{1}{2}}}^{x_{i+\frac{1}{2}}} u_j(x,t^m)dx.$$

The evolution of the cell average over a single time-step, Δt, is

$$U^{m+1}_{j,i} = U^m_{j,i} - \frac{1}{\Delta x}\left((\mathcal{F}_j)^m_{i+\frac{1}{2}} - (\mathcal{F}_j)^m_{i-\frac{1}{2}}\right) \tag{6}$$

where the numerical flux across the cell interface in arc j is given by

$$(\mathcal{F}_j)^m_{i+\frac{1}{2}} = \int_{t^m}^{t^{m+1}} f(u_j(x_{i+\frac{1}{2}}, s))ds. \tag{7}$$

Remark 2.1. *The equivalent formulation of equation* (6) *is:*

$$U^{m+1}_{j,i} = U^m_{j,i} - \frac{\Delta t}{\Delta x}\left((\mathcal{F}_j)^m_{i+\frac{1}{2}} - (\mathcal{F}_j)^m_{i-\frac{1}{2}}\right)$$

where

$$(\mathcal{F}_j)_{i+\frac{1}{2}} = \frac{1}{\Delta t}\int_{t^m}^{t^{m+1}} f(u_j(x_{i+\frac{1}{2}}, s))ds.$$

which is referred to as the temporal integral average of $f(u(x,t))$ at $x_{i+1/2}$ [40].

In Godunov's method [25] $(\mathcal{F}_j)^m_{i+\frac{1}{2}} = \mathcal{F}_j(U^m_{j,i},\ U^m_{j,i+1})$ in which the exact solution to a Riemann problem posed at the cell boundary $i+\frac{1}{2}$ is used to define the numerical flux $(\mathcal{F}_j)^m_{i+\frac{1}{2}}$. Thus in the original Godunov's method a piecewise constant reconstruction

$$u_j(x,t^m) = \sum_i U^m_{j,i}\ \ \chi_{[x_{i-\frac{1}{2}}, x_{i+\frac{1}{2}}]}(x), \tag{8}$$

where the characteristic function $\chi(x)$ is defined in the usual way as

$$\chi_{[x_{i-\frac{1}{2}}, x_{i+\frac{1}{2}}]}(x) = \begin{cases} 1, & \text{if } x \in [x_{i-\frac{1}{2}}, x_{i+\frac{1}{2}}] \\ 0, & \text{otherwise,} \end{cases}$$

was applied as a numerical approximation for $u_j(x,t)$ at time t^m.

To generalize Godunov's method, the piecewise constant approximation (8) of the solution can be replaced by a more accurate representation. In this paper, we consider a piecewise linear approximation. Thus the reconstruction in (8) takes the form

$$u_j(x,t^m) = \sum_i P_i(x,t^m;U^m_{j,\cdot})\ \ \chi_{[x_{i-\frac{1}{2}}, x_{i+\frac{1}{2}}]}(x), \tag{9}$$

where $P_i(x,t^m;U^m_{j,\cdot})$ is a linear reconstruction in cell $\mathcal{I}_i$ using data $\{U^m_{j,\cdot}\}$ in arc j such that

$$P_i(x,t^m;U^m_{j,\cdot}) = U^m_{j,i} + \sigma^m_{j,i}(x - x_i)$$

for $x \in \mathcal{I}_i$. The slope $\sigma^m_{j,i}$ in cell $\mathcal{I}_i$ is also based on the data $\{U^m_{j,\cdot}\}$. Note that $\sigma^m_{j,i} = 0$ recovers the first-order Godunov method.

To reduce oscillations, a slope limiter is applied to $\sigma_{j,i}^m$ [36]. A simple choice of slopes is the so called minmod slope:

$$\sigma_{j,i}^m = \frac{1}{\Delta x}\text{minmod}(U_{j,i+1}^m - U_{j,i}^m, U_{j,i}^m - U_{j,i-1}^m)$$

where the minmod function is defined as:

$$\begin{aligned}\text{minmod}(a,b) &= \begin{cases} a, & \text{if } |a| < |b| \text{ and } ab > 0; \\ b, & \text{if } |b| < |a| \text{ and } ab > 0; \\ 0, & \text{if } ab \leq 0; \end{cases} \\ &= \frac{1}{2}(\text{sgn}(a) + \text{sgn}(b))\min(|a|, |b|).\end{aligned}$$

It can be noted that, just as in first-order Godunov method, a Riemann problem needs to be solved at the cell boundaries $x_{i+1/2}$ since the reconstruction provides two values at the cell interfaces $x_{i+1/2}$ which we denote by

$$u_j(x_{i+\frac{1}{2}}^-, t^m) = U_{j,i-}^m; \qquad u_j(x_{i+\frac{1}{2}}^+, t^m) = U_{j,i+}^m$$

which are values based on the polynomial $P_i(x)|_{x=x_{i+\frac{1}{2}}}$ on the left of the interface and $P_{i+1}(x)|_{x=x_{i+\frac{1}{2}}}$ on the right of the interface, respectively.

The coupling condition (3) at the vertex induces a boundary condition for equation (1) at $x = 0$. At time t^m the cell averages in the first cell $i = 0$ of the connected arcs j are given by $U_{j,0}^m$ for all arcs $j = 1, \ldots, n$. Assume that they are sufficiently close to $\hat{u}_j$ such that condition (4) holds. Denote the $\kappa-$th Lax curve through the state u_0 for $\kappa = 1, 2.$ by $s \to \mathcal{L}_\kappa(u_o, s)$. Then solve for $(s_1^*, \ldots, s_n^*)$ using, for example, Newton's method the nonlinear system

$$\Psi\left(\mathcal{L}_2(U_{1,0}^m, s_1), \ldots, \mathcal{L}_2(U_{n,0}^m, s_n)\right) = 0. \tag{10}$$

A unique solution exists due to (4). The boundary value $U_{j,0}^{m+1}$ at time t^{m+1} is then given by equation (6) for $i = 0$ and with

$$U_{j,-1}^m := \mathcal{L}_2(U_{j,0}^m, s_j^*),\ j \in \{1, \ldots, n\}. \tag{11}$$

This construction yields a first–order approximation to the coupling condition and the solution u_j.

In order to obtain at least a first–order convergent scheme, we consider a *reconstruct, evolve and average algorithm* [34]. The finite–volume formulation of equation (1) is given by equation (6) and equation (7). We proceed as follows:

STEP1 Given the cell averages $U_{j,i}^m$, we reconstruct a piecewise linear function $u_j(x, t^m)$ on each cell $[x_{i-\frac{1}{2}}, x_{i+\frac{1}{2}}]$. This is a standard procedure and more details can be found, for example, in [30, 41]. We apply a reconstruction with slopes obtained by the minmod limiter for the cells $i = 1, \ldots,$ as discussed for equation (9) above.

In the first cell $i = 0$, we modify the reconstruction of the slope due to the absence of cell averages beyond the vertex since

$$\sigma_{j,0}^m = \frac{1}{\Delta x}\text{minmod}(U_{j,1}^m - U_{j,0}^m, U_{j,0}^m - U_{j,-1}^m).$$

Instead, for $U^m_{j,-1}$ the procedure applied for the first-order case can be applied here, see equation (11).

Denote the vector of the recovered slopes for both components by $\sigma_{j,i} = (\sigma^1_{j,i}, \sigma^2_{j,i})$ for $i > 0$. Using the above construction, we obtain the reconstruction

$$u_j(x, t^m) = \sigma_{j,i}(x - x_i) + U^m_{j,i}, \qquad x_{i-\frac{1}{2}} \le x \le x_{i+\frac{1}{2}},\ i = 1, \dots, \tag{12}$$

The previous reconstruction provides two values at the cell interfaces $x_{i+\frac{1}{2}}$ denoted in the following by $x_{i+\frac{1}{2}}\mp$ for the reconstruction at $x_{I+\frac{1}{2}}$ from cell i and $i+1$, respectively.

STEP2 Reconstruct for each arc j a piecewise linear function $v_j(t)$ for $t^m \le t \le t^{m+1}$ such that

$$\Psi(v_1(t^m), \dots, v_n(t^m)) = 0.$$

and

$$\frac{d}{dt}\Psi(v_1(t), \dots, v_n(t))|_{t=t^m} = 0.$$

STEP3 Evaluate equation (7) using a predictor–corrector step [35] for all cells except for $i = 0$. This approach is also attributed to Hancock in [40, 41]. We split the flux as in a Lax–Friedrichs scheme

$$f(u) = f^+(u) + f^-(u) := \frac{1}{2}\left(f(u) + au\right) + \frac{1}{2}\left(f(u) - au\right)$$

where $a = \lambda_{\max}$. Due to splitting the wave speeds of the fluxes $f(u) \pm au$ do not change sign across $x_{i+\frac{1}{2}}$. Using this fact and the midpoint rule at time $t^{m+\frac{1}{2}} = t^m + \frac{\Delta t}{2}$, the evolution of the flux (7) is given by

$$(\mathcal{F}_j)_{i+\frac{1}{2}} = \Delta t\ \left(f^+(u_j(x_{i+\frac{1}{2}}-, t^{m+\frac{1}{2}}) + f^-(u_j(x_{i+\frac{1}{2}}+, t^{m+\frac{1}{2}})\right) + O((\Delta t)^3).$$

Using Taylor expansion and the linear reconstruction (12), we obtain up to second order in space and time

$$\begin{aligned} U^m_{j,i-} &:= U^m_{j,i} + \sigma_{j,i}\frac{\Delta x}{2},\ U^m_{j,i+} := U^m_{j,i+1} - \sigma_{j,i+1}\frac{\Delta x}{2}, \\ \frac{1}{\Delta x}(\mathcal{F}_j)_{i+\frac{1}{2}} &\approx \frac{\Delta t}{\Delta x}\Big(f^+\left(U^m_{j,i-} - \frac{\Delta t}{2}Df(U^m_{j,i-})\sigma_{j,i}\right) + \\ &\qquad f^-\left(U^m_{j,i+} - \frac{\Delta t}{2}Df(U^m_{j,i+})\sigma_{j,i+1}\right)\Big). \end{aligned}$$

STEP4 Evaluate the fluxes in cell $i = 0$. The only flux which needs to be evaluated is $(\mathcal{F}_j)_{-\frac{1}{2}}$. Due to the construction of the boundary conditions in STEP2 the characteristic speed of information is non–negative. Therefore,

$$(\mathcal{F}_j)_{-\frac{1}{2}} = \int_{t^m}^{t^{m+1}} f(u_j(x_{-\frac{1}{2}}, s))ds \approx \int_{t^m}^{t^{m+1}} f(v_j(s))ds = \Delta t f(v_j(t^{m+\frac{1}{2}})) + O((\Delta t)^3).$$

Similarly, to STEP3 we evaluate

$$\frac{1}{\Delta x}(\mathcal{F}_j)_{-\frac{1}{2}} \approx \frac{\Delta t}{\Delta x} f\left(v_j(t^m) + \frac{\Delta t}{2}\frac{d}{dt}v_j(t)|_{t=t^m}\right). \tag{13}$$

STEP5 Evolve the dynamics according to equation (6) for $i = 1, \dots,$ to obtain the new cell averages at time t^{m+1} and proceed with STEP1.

To approximate the slopes $\sigma_{j,0}$ we first calculate the p.w. constant information $U_{j,-1}$ as given by (11). This data can now be used to gain the $\sigma_{j,0}$ in the usual manner (see STEP1). This approach preserves the Total variation diminishing-property of the scheme.

The difference to a standard first–order method is STEP2 and STEP3. In order to determine the values $v_j(t^m)$, we proceed similarly to the discussion in equation (10). However, since we reconstruct the function $u_j(x, t^m)$ on arc j by a piecewise linear function, the value of $u_j(x, t^m)$ closest to the vertex at time t^m is given by

$$u_j(x_{-\frac{1}{2}}, t^m) = U^m_{j,0} - \frac{\Delta x}{2}\sigma_{j,0}.$$

Hence, we determine the vector $s = (s_1, \dots, s_n) \in \mathbb{R}^n$ by solving the possibly nonlinear equation (14).

$$\Psi\left(\mathcal{L}_2(U^m_{1,0} - \frac{\Delta x}{2}\sigma_{1,0}, s_1), \dots, \mathcal{L}_2(U^m_{n,0} - \frac{\Delta x}{2}\sigma_{n,0}, s_n)\right) = 0. \tag{14}$$

For $U^m_{j,0}$ sufficiently close to $\hat{u}$ and due to condition (4), the previous equation has a unique solution s. Hence we define

$$v_j(t^m) := \mathcal{L}_2(U^m_{j,0} - \frac{\Delta x}{2}\sigma_{j,0}, s_j). \tag{15}$$

For the reconstruction in equation (13), we additionally need at least to recover also the slope $\frac{d}{dt}v_j(t)$ at time $t = t^m$. Condition (3) is supposed to hold true also for $t \geq t^m$. Hence, we obtain for sufficiently smooth solutions

(16)

$$0 = \frac{d}{dt}\Psi(u_1(0+,t), \dots, u_n(0+,t)) = \sum_{k=1}^{n} D_{u_k}\Psi\left(u_1(0+,t), \dots, u_n(0+,t)\right)\partial_t u_k(0+,t).$$

In a neighborhood of $\hat{u}$ the eigenvalues have a sign and, therefore, only a part of the information of $\partial_t u_k(0+,t)$ is available at the vertex. Further, due to (15) we will have waves emerging from the vertex in short time. Therefore, in of $D_{u_k}\Psi(u_1(0+,t), \dots, u_n(0+,t))$ we have $u_k(0+,t) = v_k(t)$ for $t > t^m$. We now approximate $\partial_t u_k(0+,t)$ for $t > t^m$ using a Roe–type scheme and compute the derivative A_j of f at the new position $v_j(t^m)$. Let the *constant* matrix A_j be defined by

$$A_j := Df(v_j(t^m)),\ j = 1, \dots, n.$$

Since f is strictly hyperbolic and for $v_j(t^m)$ in the neighborhood of $\hat{u}$, each A_j is diagonalizable with eigenvalues $\lambda^1_j < 0$ and $\lambda^2_j > 0$ and corresponding linearly independent set of eigenvectors $r_{j,1} = r_1(v_j(t^m))$ and $r_{j,2} = r_2(v_j(t^m))$, respectively. Let $R_j := (r_{j,1}, r_{j,2})$.

For small values of $t - t^m \geq 0$, we approximate $u_j(0+, t)$ by a decomposition in eigenvectors

$$u_j(t, 0+) \approx \mathbf{v}_j^1(t)\, r_{j,1} + \mathbf{v}_j^2(t)\, r_{j,2} =: R_j \begin{pmatrix} \mathbf{v}_j^1(t) \\ \mathbf{v}_j^2(t) \end{pmatrix}, \tag{17}$$

Further, we approximate the dynamics of $\partial_t \mathbf{v}_{j,1}(t)$ for small $t - t^m$ by

$$\partial_t \mathbf{v}_j^1(t^m) = -\lambda_j^1 \partial_x \left(R_j^{-1} u_j(t^m, 0+) \right)^1 = -\lambda_j^1 \left(R_j^{-1} \begin{pmatrix} \sigma_{j,0}^1 \\ \sigma_{j,0}^2 \end{pmatrix} \right)^1. \tag{18}$$

where we used the linear reconstruction of $u_j(x, t)$ on arc j and the super–index denotes the component $\in \{1, 2\}$ of the vector. Then, we obtain from equation (16) at time t^m an equation in the unknowns $\mathbf{v}_j^2$

$$0 = \sum_{k=1}^{n} D_k \Psi(v_1(t^m), \ldots, v_n(t^m)) R_j \begin{pmatrix} \mathbf{v}_j^1(t) \\ \mathbf{v}_j^2(t) \end{pmatrix}$$

or equivalently

$$\sum_{k=1}^{n} D_k \Psi(v_1(t^m), \ldots, v_n(t^m)) r_1(v_k(t^m) \lambda_k^1 \left(R_k^{-1} \begin{pmatrix} \sigma_{k,0}^1 \\ \sigma_{k,0}^2 \end{pmatrix} \right)^1 = \tag{19}$$

$$\sum_{k=1}^{n} D_k \Psi(v_1(t^m), \ldots, v_n(t^m) r_2(v_k(t^m) \partial_t \mathbf{v}_k^2(t^m) \tag{20}$$

Again, due to condition (4) the previous equation (19) has a unique solution for the n values $\partial_t \mathbf{v}_j^2(t^m)$, $j = 1, \ldots, n$. Then, we set

$$\frac{d}{dt} v_j(t^m) := \sum_{\ell=1}^{2} \partial_t \mathbf{v}_j^\ell(t^m) r_\ell(v_j(t^m)). \tag{21}$$

A piecewise linear reconstruction of v_j yields at time $t = t^m$

$$\Psi \left(v_1(t^m) + \frac{d}{dt} v_1(t^m)(t - t^m), \ldots, v_n(t^m) + \frac{d}{dt} v_n(t^m)(t - t^m) \right) = O((t - t^m)^2).$$

We summarize the computations in the following Lemma.

Lemma 2.2. *Consider a single node with n connected arcs and let t^m be some positive time. Let $\Psi \in C^2(\mathbb{R}^{2n}; \mathbb{R}^n)$ and let $\hat{u}_j := U_{j,0}^m - \frac{\Delta x}{2}$ be such that equation (4) holds true. Then, for $v_j(t)$ as in the previous construction, the coupling condition is satisfied up to second order in time, i.e.*

$$\Psi\left(v_1(t), \ldots, v_n(t)\right) = O((t - t^m)^2).$$

3. Properties of the scheme in the linear case

In order to illustrate the properties of the scheme, we first consider the case of a single arc extending from $-\infty$ to ∞. We drop for a moment in the index j. Also, assume that $u \in \mathbb{R}$, $f : \mathbb{R} \to \mathbb{R}$ and is given by

$$f(u) = c\, u,\ c > 0. \tag{22}$$

Since $a = c$, we obtain $f^+(u) = cu$, $f^-(u) = 0$ and $Df^{\pm}(u) = \frac{1}{2}(c \pm a)$. The CFL condition gives $c\Delta t \leq \Delta x$. The numerical flux at the cell boundary is then given by

$$\mathcal{F}_{i+\frac{1}{2}} = \frac{\Delta t}{\Delta x} c \left(U_i^m + \sigma_i \frac{\Delta x}{2} - \frac{c\Delta t}{2} \sigma_i \right).$$

The scheme, therefore, takes the form:

$$U_i^{m+1} = U_i^m - \frac{\Delta t}{\Delta x} c \left(U_i^m - U_{i-1}^m + \frac{\Delta x - c\Delta t}{2} (\sigma_i - \sigma_{i-1}) \right). \tag{23}$$

One easily verifies that this method is second order accurate in space and time.

Further, we consider the scalar case $n = 1$ and two connected arcs $j = 1, 2$ with $f_1(u) = -c\,u$, $f_2(u) = c\,u$ and $c > 0$. Note that this case does *not* fulfill the general assumption on the eigenvalues given previously. Therefore, we need to modify the construction slightly. However, we still want to treat this case to show its relation to a discretization of a single scalar advection equation. The coupling condition Ψ preserves the total mass and reads

$$\Psi(u_1(0+,t), u_2(0+,t)) = u_2(0+,t) - u_1(0+,t) = 0. \tag{24}$$

This situation is then equivalent to a Cauchy problem for $y(x,t)$ with combined domain $x \in \mathbb{R}$ and $t \geq 0$

$$\partial_t y(x,t) + c\partial_x y(x,t) = 0,\ y(x,0) = y_0(x) := \begin{pmatrix} u_{1,0}(-x), & \text{for } x \leq 0 \\ u_{2,0}(x), & \text{for } x > 0. \end{pmatrix}. \tag{25}$$

In the following derivations, we show that the previous construction leads to a scheme of second order (23) in space and time for equation (25). Clearly, the eigenvalues are $\lambda = -c$ and $\lambda = c$ for arcs $j = 1, 2$, respectively, and therefore for arc $j = 1$, the assumptions are *not* fulfilled. Therefore, at $x = 0$, we do not prescribe any boundary condition. Hence, a single coupling condition is sufficient to have a well–posed problem (26) and initial data (2).

$$\partial_t u_j + \partial_x f_j(u_j) = 0,\ x \geq 0,\ t \geq 0, \text{ and } u_2(0+,t) - u_1(0+,t) = 0,\ t \geq 0. \tag{26}$$

In order to use a similar notation as above, we note that the admissible boundary states for arc $j = 2$ are given by

$$\mathcal{L}_2(\hat{u}_2, s_2) = s_2 + \hat{u}_2,\ s_2 \in \mathbb{R}.$$

In arc $j = 1$, we have $\mathcal{L}_2(\hat{u}_1, s_1) = \hat{u}_1$. Hence, for the unknown s_2 the condition (14) becomes:

$$U_{1,0}^m - \frac{\Delta x}{2}\sigma_{1,0} - \left(U_{2,0}^m - \frac{\Delta x}{2}\sigma_{2,0} + s_2 \right) = 0. \tag{27}$$

and equation (15) gives:

$$v_2(t^m) = U_{1,0}^m - \frac{\Delta x}{2}\sigma_{1,0},\ v_1(t^m) = U_{1,0}^m - \frac{\Delta x}{2}\sigma_{1,0}. \tag{28}$$

We can not use condition (19) directly, since the assumptions on the sign of the eigenvalues are not fulfilled in arc $j = 1$. However, we can repeat the computations (16) to (21) and obtain, for sufficiently smooth solution $u_1(0+,t)$,

$$0 = \partial_t u_1(0+,t) - \partial_t u_2(0+,t) = +c\partial_x u_1(0+,t) - R_2 = c\,\sigma_{1,0} - R_2.$$

Here, we also used the fact that on arc $j = 1$ and for sufficiently smooth u_1, we have $\partial_t u_1(0+,t) - c\partial_x u_1(0+,t) = 0$. Therefore, the linear reconstruction of $v_2(t)$ for $t^{m+1} > t \geq t^m$ reads

$$v_2(t) = U_{1,0}^m - \frac{\Delta x}{2}\sigma_{1,0} + c\,\sigma_{1,0}(t - t^m). \tag{29}$$

The numerical flux in cell $i = 0$ is then given as

$$(\mathcal{F}_2)_{-\frac{1}{2}} = \Delta t\; c\; \left(U_{1,0}^m - \frac{\Delta x}{2}\sigma_{1,0} + \frac{\Delta t}{2}\; c\; \sigma_{1,0} \right).$$

In order to compare the proposed method with a numerical discretization of equation (25) it suffices to consider the discretization of the first cell $i = 0$ of arc $j = 2$. The remaining cells are independent of the coupling condition and therefore the applied discretization coincide. In the first cell $i = 0$ of arc $j = 2$ we obtain from (29) and (13)

$$U_{2,0}^{m+1} = U_{2,0}^m - \frac{\Delta t}{\Delta x}\; c\; \left(U_{2,0}^m - U_{1,0}^m + (\sigma_{2,0} + \sigma_{1,0})\frac{\Delta x - c\Delta t}{2} \right). \tag{30}$$

Suppose a discretization of equation (25) with $i \in \mathbb{N}$ and such that at $x = 0$ we have the location of the physical node and as before $x_i = \frac{\Delta x}{2}$ for $i = 0$ is the location of the center of the grid. The discretization (30) has to be compared with a corresponding second order discretization of equation (25) in cell $i = 0$, i.e., for $x \in [-\frac{\Delta x}{2}, \frac{\Delta x}{2}]$. Using equation (23) we obtain for the cell averages $Y_i^m = \dfrac{1}{\Delta x}\displaystyle\int_{x_{i-\frac{1}{2}}}^{x_{i+\frac{1}{2}}} y(x,t^m)dx$

$$Y_0^{m+1} = Y_0^m - \frac{\Delta t}{\Delta x} c \left(Y_0^m - Y_{-1}^m + (\tau_0 - \tau_{-1})\,\frac{\Delta x - c\Delta t}{2} \right). \tag{31}$$

The construction of $\sigma_{2,0}$ and τ_0 are independent of the coupling condition and therefore $\sigma_{2,0} = \tau_0$. In the continuous case we have $y(-x,t) = u_1(x,t)$ and therefore $Y_i^m = U_{1,-i+1}^m$ for $i < 0$ and the slopes of the linear reconstruction of y and u_1 are related as $\sigma_{1,-i} = -\tau_{i+1},\ i < 0$. Hence, provided we use the same derivation of the slopes for $U_{j,i}$ and Y_i we observe that the proposed discretization of the coupling condition leads to the same scheme as a discretization for the Cauchy problem (25). In particular, the coupling condition does *not* lead to an order reduction. We summarize the findings in the following Lemma.

Lemma 3.1. *Let $n = 2$ and consider for $(x,t) \in \mathbb{R}_0^+ \times \mathbb{R}^+$ the problem*

$$\partial_t u_1 + c\partial_x u_1 = 0,\ \partial_t u_2 - c\partial_x u_2 = 0,$$

with initial data given by (2) *and coupling condition* (24)*. On an equidistant spatial grid $(x_i), i \in \mathbb{N}$ consider a piecewise linear reconstruction $u_j(x,t^m)$ for $j = 1,2$. Consider furthermore the second–order MUSCL discretization* (31) *of equation* (25) *with initial data at time $t = t^m$ given by $y(x,t^m) = u_j(-x,t^m)H(-x) + u_j(x,t^m)H(x)$.*

Then, for $c = a$ and $j \geq 0$, the cell averages $U_{1,j}^{m+1}$ and $U_{2,j}^{m+1}$ obtained from the proposed algorithm coincide with the cell averages Y_{-j-1}^{m+1} and Y_j^{m+1}, respectively.

Next, we consider the case of a linear system $f(u) = Au$ with $A \in \mathbb{R}^2$ strictly hyperbolic with $\lambda_1 < 0$ and $\lambda_2 > 0$. We denote by $R = (r_1, r_2)$ the matrix of the (right)

eigenvectors to A. Further, consider the case of a *single* arc $n = 1$. Then, problem (1) – (3) is a boundary value problem for $u_1(x,t)$ with $x \geq 0$ and boundary conditions induced by equation (3). We prescribe as boundary condition $t \to b(t), b \in C^1$, in the second characteristic variable. In terms of Ψ, we obtain

$$\Psi(u_1(0+,t)) = (R^{-1}u_1(0+,t))^2 - b(t). \tag{32}$$

On the time interval (t^m, t^{m+1}) we expect the linear construction in the second component $v_1(t) \in \mathbb{R}^2$ to be

$$v(t) = R\left(\left(R^{-1}\left(u_1(0+,t^m) + \partial_t u_1(0+,t^m)\right)\right)^1,\ b(t^m) + b'(t^m)(t-t^m)\right)^T + O((t-t^m)^2).$$

We compare the presented approach to the approach presented in [5]. Due to the linearity of A, we have for any $\hat{u} \in \mathbb{R}^2$

$$\mathcal{L}_2(\hat{u}, s) = \hat{u} + s\ r_2. \tag{33}$$

At first we discuss the reconstruction of STEP2. Due to the linear reconstruction in each cell, we have $U^m_{1,0} - \frac{\Delta x}{2}\sigma_{1,0} = u_1(0+,t^m) + O(\Delta x)^2$. Equation (14), (15) and (32) yield

$$\begin{aligned}
0 = \Psi(\mathcal{L}_2(U^m_{1,0} - \frac{\Delta x}{2}\sigma_{1,0}, s_1)) &= \left(R^{-1}\left(U^m_{1,0} - \frac{\Delta x}{2}\sigma_{1,0} + s_1 r_2\right)\right)^2 - b(t^m) \\
&= \left(R^{-1}(U^m_{1,0} - \frac{\Delta x}{2}\sigma_{1,0})\right)^2 + s_1 - b(t) \\
v_1(t^m) = U^m_{1,0} - \frac{\Delta x}{2}\sigma_{1,0} + s_1\ r_2 & \\
&= R\left(R^{-1}(U^m_{1,0} - \frac{\Delta x}{2}\sigma_{1,0})\right) + b(t^m)r_2 - \left(R^{-1}(U^m_{1,0} - \frac{\Delta x}{2}\sigma_{1,0})\right)^2 R\begin{pmatrix}0\\1\end{pmatrix} \\
&= R\left(R^{-1}(U^m_{1,0} - \frac{\Delta x}{2}\sigma_{1,0}) - \left(R^{-1}(U^m_{1,0} - \frac{\Delta x}{2}\sigma_{1,0})\right)^2\begin{pmatrix}0\\1\end{pmatrix}\right) + R\begin{pmatrix}0\\b(t^m)\end{pmatrix} \\
&= R\begin{pmatrix}(R^{-1}u_1(0+,t^m))^1 + O(\Delta x)^2 \\ b(t^m)\end{pmatrix}.
\end{aligned}$$

The slope $\frac{d}{dt}v_1(t^m)$ is computed using equation (16) to (21). Equation (16) reads

$$0 = (R^{-1}\partial_t u_1(0+,t))^2 - b'(t), \tag{34}$$

and we approximate $\partial_t u_1(0+,t)$ by decomposition in characteristic variables to obtain

$$\partial_t \mathbf{v}^1_1(t^m) = -\lambda^1\left(R^{-1}\sigma_{1,0}\right)^1 = \left(R^{-1}\partial_t u_1(0+,t^m)\right)^1 + O(\Delta x)^2.$$

and according to (19) at time t^m

$$\begin{aligned}
0 &= \left(R^{-1}\left(\left(R^{-1}\partial_t u_1(0+,t^m)\right)^1 r_1 + \partial_t \mathbf{v}^2_1(t^m) r_2\right)\right)^2 - b'(t^m) \\
&= \partial_t \mathbf{v}^2_1(t^m) - b'(t^m).
\end{aligned}$$

Due to (21), we obtain for $t - t^m = O(\Delta x)$ the reconstruction

$$\begin{aligned} v_1(t) &= R \begin{pmatrix} (R^{-1} u_1(0+, t^m))^1 \\ b(t^m) \end{pmatrix} + (t - t^m) \left(b'(t^m) r_2 + \left(R^{-1} \partial_t u_1(0+, t^m) \right)^1 r_1 \right) \\ &= R \begin{pmatrix} \left(R^{-1} \left(u_1(0+, t^m) \right)^1 + (t - t^m) \partial_t u_1(0+, t^m) \right) \big)^1 + O(\Delta x)^2 \\ b(t^m) + (t - t^m) b'(t^m) \end{pmatrix}. \end{aligned} \tag{35}$$

In [5] the following approach has been proposed to obtain a high order reconstruction of $v_1(t)$. We apply this procedure to a first–order scheme studied herein. The derivation of $v_1(t^m)$ is as above. However, there is a difference in the approximation of the derivative $\partial_t v_1(t^m)$. Instead of a characteristic decomposition, the value of the derivative is approximated using the Lax–curve to the linearized system, i.e.,

$$\mathcal{L}_2(\partial_t u_1(0+, t), s_1'(t)) = \partial_t u_1(0+, t) + s_1'(t) r_2,$$

and the (real valued) unknown $s_1'(t)$ at time $t = t^m$ is obtained as solution to equation (34). In order to evaluate $\partial_t u_1(0+, t)$ the linearized equation, i.e., $\partial_t u_1(0+, t^m) = -\begin{pmatrix} \lambda^1 & 0 \\ 0 & \lambda^2 \end{pmatrix} \sigma_{1,0}$ is used leading to an error of order $O(\Delta x)^2$ due to the spatial reconstruction of $u_1(x, t)$. Hence,

$$0 = \left(R^{-1} \partial_t u_1(0+, t) \right)^2 - b'(t^m) + s_1'(t^m) \left(R^{-1} r_2 \right)^2 + O(\Delta x)^2$$

Finally, the reconstruction of $v_1(t)$ up to second order in time is given by

$$\begin{aligned} v_1(t) &= R \begin{pmatrix} (R^{-1} u_1(0+, t^m))^1 \\ b(t^m) \end{pmatrix} + (t - t^m) \mathcal{L}_2(\partial_t u_1(0+, t), s_1'(t)) \\ &= R \begin{pmatrix} \left(R^{-1} (u_1(0+, t^m) + (t - t^m) \partial_t u_1(0+, t^m)) \right)^1 + O(\Delta x)^2 \\ b(t^m) + b'(t^m)(t - t^m) + O(\Delta x)^2 \end{pmatrix} \end{aligned} \tag{36}$$

In characteristic variables $Rv_1(t)$, the difference of (35) and (36) is of order $O(\Delta x)^2$ in the recovered boundary condition. This is an error of the order of the scheme. However, in the presented approach *no* information on $(R \partial_t u_1(0+, t))^2$ (being the outgoing characteristic) is needed and for small Δt the resolution of $b(t)$ is of order $\frac{\Delta t^2}{2}$ instead of order $(\Delta x)^2 = \lambda_{\max}^2 (\Delta t)^2$.

The previous relation also holds true in a more general setting: Consider n connected arcs and denote the state at $x = 0+$ on arc k by $\hat{u}_k = U_{k,0}^m - \frac{\Delta x}{2} \sigma_{k,0}$. Denote by $A_k = Df(\hat{u}_k)$ and by $R_k = (r_{k,1}, r_{k,2})$ the matrix of (right) eigenvectors of A_k. The superscript in u^ℓ denotes the component ℓ of the respective vector u. Let $\hat{u}_{k,t}$ be $\hat{u}_{k,t} := -A \sigma_{k,0} = \partial_t \hat{u}_k(0+, t^m) + O(\Delta x)^2$ and let $\Psi : \mathbb{R}^{2n} \to \mathbb{R}^n$ be a C^1 function with partial derivatives $\Psi_{u_k} := D_{u_k} \Psi(\hat{u})$. Then, [5] requires to solve the following system for $\xi = (\xi_k)_k \in \mathbb{R}^n$ and reconstruct $v(t) \in \mathbb{R}^n$ by

$$0 = \sum_{k=1}^{n} \Psi_{u_k} \left(\hat{u}_{k,t} + \xi_k r_{k,2} \right),$$

$$\frac{d}{dt} v_k(t^m) := \hat{u}_{k,t} + \xi_k r_{k,2}.$$

Due to condition (4) the matrix $\mathcal{A} \in \mathbb{R}^{n\times n}$ defined by

$$\mathcal{A} = (\Psi_{u_1} r_{1,2}, \dots, \Psi_{u_n} r_{n,2})$$

is invertible and we obtain for the second component of $\frac{d}{dt} v_j(t^m)$ and $\xi_j = \left(\sum_{k=1}^{n} \mathcal{A}^{-1} \Psi_{u_k} \hat{u}_{k,t} \right)^j$ the following equivalence

$$\begin{aligned}
\left(R_j^{-1} \frac{d}{dt} v_j(t^m) \right)^2 &= \left(R_j^{-1} \hat{u}_{j,t} \right)^2 - \xi_j \left(R_j^{-1} r_{j,2} \right)^2 \\
&= \left(R_j^{-1} \hat{u}_{j,t} \right)^2 - \left(\sum_{k=1}^{n} \mathcal{A}^{-1} \Psi_{u_k} R_k R_k^{-1} \hat{u}_{k,t} \right)^j = \\
&= \left(R_j^{-1} \hat{u}_{j,t} \right)^2 \\
&\quad - \left(\mathcal{A}^{-1} \left(\sum_{k=1}^{n} \Psi_{u_k} r_{k,1} (R_k^{-1} \hat{u}_{k,t})^1 + \sum_{k=1}^{n} \Psi_{u_k} r_{k,2} (R_k^{-1} \hat{u}_{k,t})^2 \right) \right)^j \\
&= \left(R_j^{-1} \hat{u}_{j,t} \right)^2 - \left(\mathcal{A}^{-1} \sum_{k=1}^{n} \Psi_{u_k} r_{k,1} (R_k^{-1} \hat{u}_{k,t})^1 \right)^j \\
&\qquad - \left(\mathcal{A}^{-1} \mathcal{A} \begin{pmatrix} (R_1^{-1} \hat{u}_{1,t})^2 \\ \vdots \\ (R_n^{-1} \hat{u}_{n,t})^2 \end{pmatrix} \right)^j
\end{aligned}$$

Summarizing, we observe that the previous computation of the second component of $\frac{d}{dt} v_j(t^m)$ up to $O(\Delta x)^2$ with equation (19) and (21). Hence, the proposed method slightly improves the construction presented in [5]. Compared with [5] it also does not require during the construction information on $(R_j^{-1} \hat{u}_{j,t})^2$ being the information on the *outgoing* characteristic on arc j.

4. Application to gas dynamics

We discuss the application of the method to gas dynamics in connected pipe systems. Those problems have been studied intensively in the past years and we refer e.g. to [1, 2, 11, 13–16] for analytical and computational results. Here, we study a single node with n connected arcs and on each arc the dynamics are governed by the isentropic Euler equations (37) (or the p-system). We assume a subsonic state $\hat{u} = (\hat{u}_j)_{j=1}^n$ is given such that condition (4) is fulfilled. The wave curves and properties of the isentropic Euler equations are well known [18] and they are given on arc j by

$$0 = \partial_t \rho_j + \partial_x q_j \text{ and } 0 = \partial_t q_j + \partial_x \left(p(\rho_j) + \frac{q_j^2}{\rho_j} \right). \tag{37}$$

Here, $p(\cdot) \in C^2$ is the pressure law which is supposed to be non–negative, strictly monotone increasing and convex, with e.g. $p(\rho) = a^2 \rho$ being a model for isothermal

gas. The subsonic region is the set $\Omega := \{(\rho, q) : \rho > 0, \lambda^1(\rho, q) < 0 < \lambda^2(\rho, q)\}$ where $\lambda^{1,2} = \frac{q}{\rho} \mp \sqrt{p'(\rho)}$. The corresponding (right) eigenvectors are

$$r_1(\rho, q) = \begin{pmatrix} -1 \\ -\lambda^1(\rho, q) \end{pmatrix} \text{ and } r_2(\rho, q) = \begin{pmatrix} 1 \\ \lambda^2(\rho, q) \end{pmatrix}.$$

The reversed 2–Lax curve exiting at $(\hat\rho, \hat q)$ is given by

$$\mathcal{L}_2(\hat u, \sigma) = \begin{pmatrix} \sigma \frac{\hat q}{\hat\rho} + \sqrt{\frac{\sigma}{\hat\rho}(\sigma - \hat\rho)(p(\sigma) - p(\hat\rho))}, & \sigma > \hat\rho \\ \sigma \frac{\hat q}{\hat\rho} - \sigma \int_\sigma^{\hat\rho} \frac{\sqrt{p'(s)}}{s} ds, & \sigma \le \hat\rho \end{pmatrix}. \tag{38}$$

Different coupling conditions have been proposed in the literature [1]. Common to all is the conservation of mass flux across the node. Hence, the first component of Ψ reads

$$\Psi^1(\hat u(t, 0+)) = \sum_{j=1}^n \hat q_j(t, 0+). \tag{39}$$

The remaining $n - 1$ conditions can be prescribed for example by the equality of the pressure

$$\Psi^j(\hat u(0+, t)) = p(\hat\rho_j(0+, t)) - p(\hat\rho_{j-1}(0+, t)),\ j = 2, \dots, n. \tag{40}$$

Remark 4.1. *Let $n = 2$. Consider coupling condition* (39) *and the equality of momentum*

$$\Psi^2(\hat u(0+, t)) = p(\hat\rho_2(0+, t)) + \frac{\hat q_2^2(0+, t)}{\hat\rho_2(0+, t)} - p(\hat\rho_1(0+, t)) - \frac{\hat q_1^2(0+, t)}{\hat\rho_1(0+, t)}.$$

We recover a solution $(\bar\rho, \bar q)(x, t)$ to the Cauchy problem

$$0 = \partial_t \bar\rho + \partial_x \bar q,\ 0 = \partial_t \bar q + \partial_x \left(p(\bar\rho) + \frac{\bar q^2}{\bar\rho} \right),\ x \in \mathbb{R},\ t \ge 0,$$

by $\bar q(x, t) = -q_1(-x, t)$ and by $\bar q(x, t) = q_2(x, t)$ for $x \in \mathbb{R}_0^+$. For details we refer to [12].

For the reconstruction of $v_j(t)$ in STEP2, we collect the following elementary computations. Equation (14) is solved for $s \in \mathbb{R}^n$ using Newton's method with $\mathcal{L}_2(\hat u, s)$ given by equation (38) and Ψ given by (39) and (40), respectively. This enables us to determine $v_j(t^m)$ according to (15). In order to obtain $\partial_t v_j(t^m)$, we solve equation (18) with $R_j = (r_1(v_j(t^m)), r_2(v_j(t^m)))$. For the second component we note that

$$\begin{aligned} &(D_{u_1}\Psi(\hat u) r_2(\hat u_1), \dots, D_{u_n}\Psi(\hat u) r_2(\hat u_n)) \\ &= \begin{pmatrix} \lambda^2(\hat\rho_1, \hat q_1) & \lambda^2(\hat\rho_2, \hat q_2) & & \dots & \lambda^2(\hat\rho_n, \hat q_n) \\ -p'(\hat\rho_1) & p'(\hat\rho_2) & & & \\ & -p'(\hat\rho_2) & p'(\hat\rho_3) & & \\ & & & \ddots & \\ & & & -p'(\hat\rho_{n-1}) & p'(\hat\rho_n) \end{pmatrix}. \end{aligned}$$

Further, for $\hat{u} := (v_j(t^m))_{j=1}^n$ we compute the vector

$$\sum_{k=1}^{n} D_k\Psi(\hat{u})r_1(\hat{u}_k)\lambda^1(\hat{u}_k)\left(R_k^{-1}\sigma_{k,0}\right)^1$$
$$= \begin{pmatrix} -\lambda^1(\hat{\rho}_1,\hat{q}_1) & -\lambda^1(\hat{\rho}_2,\hat{q}_2) & & \dots & -\lambda^1(\hat{\rho}_n,\hat{q}_n) \\ p'(\hat{\rho}_1) & -p'(\hat{\rho}_2) & & & \\ & p'(\hat{\rho}_2) & -p'(\hat{\rho}_3) & & \\ & & & \ddots & \\ & & & p'(\hat{\rho}_{n-1}) & -p'(\hat{\rho}_n) \end{pmatrix} \times$$
$$\begin{pmatrix} \lambda^1(\hat{u}_1)\left(R_1^{-1}\sigma_{1,0}\right)^1 \\ \vdots \\ \lambda^1(\hat{u}_n)\left(R_n^{-1}\sigma_{n,0}\right)^1 \end{pmatrix}.$$

The previous computations enable us to solve equation (19) for $\partial_t \mathbf{v}_k^2(t^m)$ and hence to determine $\frac{d}{dt}v_j(t^m)$ by equation (21).

5. Computational results

5.1. **Linear and node vs linear on a single arc.**

Here we will show numerical results on a linear transport equation as (1) for a single arc (therefore, we drop the index j).
The setup is a periodic domain $x \in [0, 2\pi]$ (i.e. for the state u we have $u(0,t) = u(2\pi,t),\ \forall t \geq 0$), as flux we set $f \equiv 1$, and the initial condition (2) is picked as $u_o(x) = \sin(x)$.
For the nodal solution on the domain $[0, 2\pi]$ we coupled the arc with itself and we used ϕ as in (24), i.e. $\Psi(u(t,0+), u(t,2\pi-)) = u(t,0+) - u(t,2\pi-) = 0\ \forall t \geq 0$.
Furthermore, the Courant number is set to 0.9 and the following examples are grounded on a final time $T = 10$. For both scenarios we implementet a first order accurate Upwind scheme as well as a MUSCL scheme [41], where we used the modified MUSCL scheme as in (30) in the coupled case.
The following will illustrate both scheme in the spacial cyclic and in the nodal coupled case. The power k of $N_k = 2^k$ (the number of degrees of freedom of the spacial discretization) we plotted against $\frac{\log(e_{N_k})}{\log(2)}$, where e_{N_k} is the L^1 error to the analytical solution for a given N_k.
bla

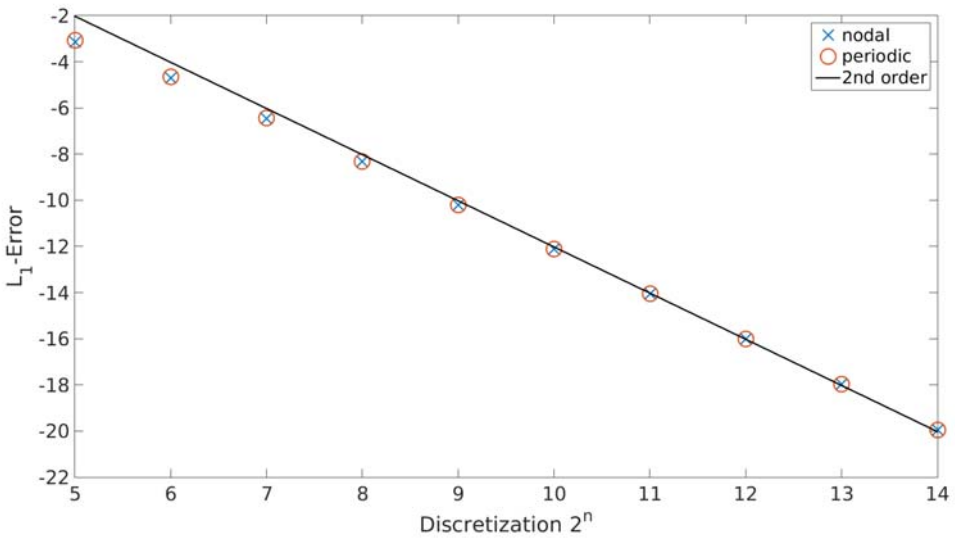

FIGURE 1. L^1 error of both, periodic boundary and nodal coupled method numerical approximation to analytical solution.

Here, table 5.1 contains the L^1 errors and convergence rate of the upper plots. N_k and $r_k = \frac{\log(e_{N_k})}{\log(2)}$ as above. The "Rate" columns are therefore $r_k - r_{k+1}$ of each error.

N_k	Upwind r_k	Rate	MUSCL periodic r_k	Rate	MUSCL nodal r_k	Rate
2^5	-0.7428	/	-3.0768	/	-3.1472	/
2^6	-1.5442	0.8014	-4.6573	1.5805	-4.7055	1.5583
2^7	-2.4380	0.8938	-6.4464	1.7891	-6.4689	1.7635
2^8	-3.3842	0.9462	-8.3080	1.8616	-8.3198	1.8509
2^9	-4.3577	0.9735	-10.1955	1.8876	-10.2018	1.8820
2^{10}	-5.3440	0.9863	-12.1139	1.9184	-12.1171	1.9153
2^{11}	-6.3372	0.9932	-14.0533	1.9394	-14.0549	1.9378
2^{12}	-7.3339	0.9967	-16.0073	1.9540	-16.0081	1.9532
2^{13}	-8.3322	0.9983	-17.9715	1.9642	-17.9719	1.9638
2^{14}	-9.3313	0.9991	-19.9429	1.9714	-19.9431	1.9712

TABLE 1. Comparison of convergence of the periodic boundary to the nodal coupled method

5.2. **Gas dynamics.** We compute the conservation law given by equation (37). As above, we have a spatial domain $x \in [0, 2\pi]$ with $u(0,t) = u(2\pi,t)\ \forall\ t \geq 0$ and we are going to couple this arc with itself. We compare the results with a second order MUSCL scheme on a periodic domain. As first component of the coupling Ψ the conservation of mass (39) is used. For the second component we employ the conservation of momentum

as suggested in Remark 4.1. The second condition leads to a true nonlinear coupling compared with the approach by [5]. There, a linear coupling is used.

Further note that we are connecting the states of the arc at spatial coordinates $x = 0$ and $x = 2\pi$. Therefore we have to alter the notion on the Lax-curves. At $x = 0$ we use the second Lax-curve at stated in (10). In contrast to this at $x = 1$ we have to employ the first Lax-curve. A parametrization of this can be found in [1].

The initial data we set are

$$U(x,0) = \begin{pmatrix} \rho(x,0) \\ q(x,0) \end{pmatrix} = \begin{pmatrix} 0.1\cos(x) + 1 \\ 0.05\cos(x) + 2 \end{pmatrix}. \tag{41}$$

The final time is $T = 0.4$ (to prevent shocks from happening to recover the second order accuracy of the scheme). The chosen pressure law is

$$p(\rho) = a^2\rho \text{ and } a = 5.$$

Again a MUSCL scheme is used as in Section 2 suggested. We can compare the periodic standard second order solution $U_{cyc} = (\rho_{cyc}, q_{cyc})^\top$ to the coupled solution $U_{cc} = (\rho_{cc}, q_{cc})^\top$.

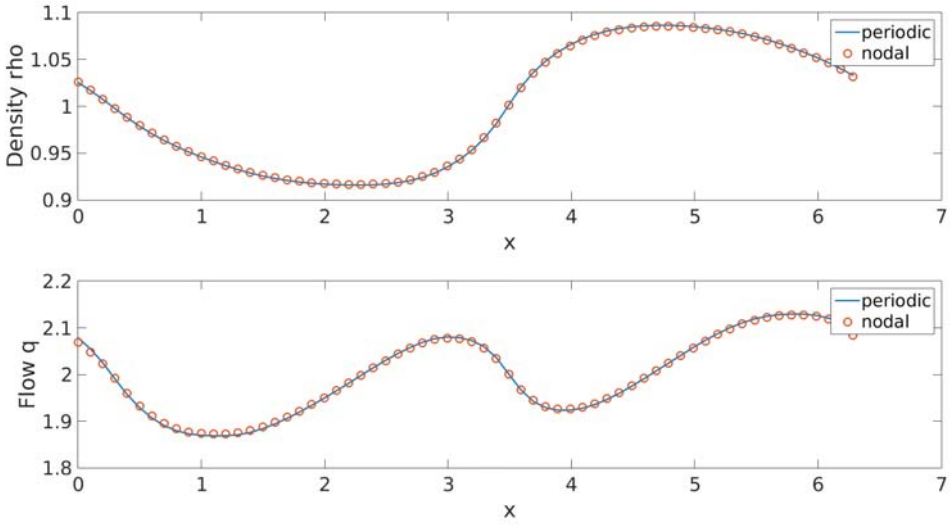

FIGURE 2. Periodic versus nodal coupled solution

The Table 5.2 contains the L^1 errors and convergence rate of the coupled solution compared to the periodic case. $N_k = 2^k$ is the number of degrees of freedom due to the spatial discretization. The column "L^1 ρ" gives $r_{\rho_k} = \log(\|\rho_{cyc} - \rho_{cc}\|_{L^1})/\log(2)$ and "L^1 q" $r_{q_k} = \log(\|q_{cyc} - q_{cc}\|_{L^1})/\log(2)$ analogously. The "Rate" columns are therefore $r_k - r_{k+1}$ of each error of both quantities ρ and q.

N_k	L^1 ρ	L^1 q	Rate ρ	Rate q
2^5	-8.8259	-7.1826	/	/
2^6	-10.4556	-8.6067	1.6297	1.4242
2^7	-12.1436	-10.3566	1.6880	1.7499
2^8	-13.8907	-12.1301	1.7471	1.7735
2^9	-15.6996	-13.9506	1.8089	1.8205
2^{10}	-17.5927	-15.8745	1.8931	1.9239
2^{11}	-19.5538	-17.8503	1.9611	1.9758
2^{12}	-21.5445	-19.8373	1.9907	1.9870

TABLE 2. L^1 convergence of the periodic boundary to the nodal coupled method

The Table 5.2 contains the L^∞ errors and convergence rate of the coupled solution. The scenario is the same as in Table 5.2 but all data are presented under the L^∞ norm. We observe here, that the scheme is first order only. This is due to the local first order accuracy of the TVD method at a local extremum (as reasoned in chapter 4 of [24]).

N_k	L^∞ ρ	L^∞ ρ	Rate ρ	Rate q
2^5	-8.1963	-5.1755	/	/
2^6	-9.2077	-6.1543	1.0114	0.9788
2^7	-10.1478	-7.1371	0.9402	0.9828
2^8	-10.9934	-8.0115	0.8456	0.8745
2^9	-11.9733	-9.0249	0.9799	1.0134
2^{10}	-13.0005	-10.0815	1.0272	1.0566
2^{11}	-13.9772	-11.0764	0.9767	0.9948
2^{12}	-14.9497	-12.0575	0.9725	0.9811

TABLE 3. L^∞ convergence of the periodic boundary to the nodal coupled method

5.3. **Gas dynamics – Y-junction.** Here we have a look at the setup as suggested in Section 2 for $n = 3$ (number of arcs attatched to the node at $x = 0$). Obviously, in the numerics we cannot extend the arcs to infinity. Therefore we consider a finite spatial domain, which will be $x \in [0, 2]$ for all arcs. For the boundary which is not adjacent to the coupled knot we implemented Neumann boundary conditions. The chosen coupling conditions are the conservation of mass (39) and conservation of momentum 4.1.

The initial data are as follows:
For the first arc $j = 1$ we set

$$U_1(x, 0) = \begin{pmatrix} \rho_1(x, 0) \\ q_1(x, 0) \end{pmatrix}$$

with

$$\rho_1(x, 0) = \begin{cases} -x^3 + \frac{3}{2}x^2 + 1 & x \in [0, 1) \\ \frac{3}{2} & x \in [1, 2] \end{cases}$$

and

$$q_1(x,0) = \begin{cases} -x^3 + \frac{3}{2}(x-1)^2 & x \in [0,1) \\ \frac{1}{2} & x \in [1,2] \end{cases}.$$

For $j = 2, 3$ we have

$$U_j(x,0) = \begin{pmatrix} \rho_j(x,0) \\ q_j(x,0) \end{pmatrix}$$

with

$$q_j(x,0) \equiv 0$$

and

$$\rho_j(x,0) \equiv 1.$$

Those initial data are smooth and give us a feasible initial state with respect to the coupling condition. Hence, $\Psi(U_1(x,0), U_2(x,0), U_3(x,0)) = (0,0,0)^\top$.

The chosen pressure law is again

$$p(\rho) = a^2\rho \text{ and } a = 5$$

and the final time is set to $T = 0.3$. The remaining numerics is the same as in 5.2.

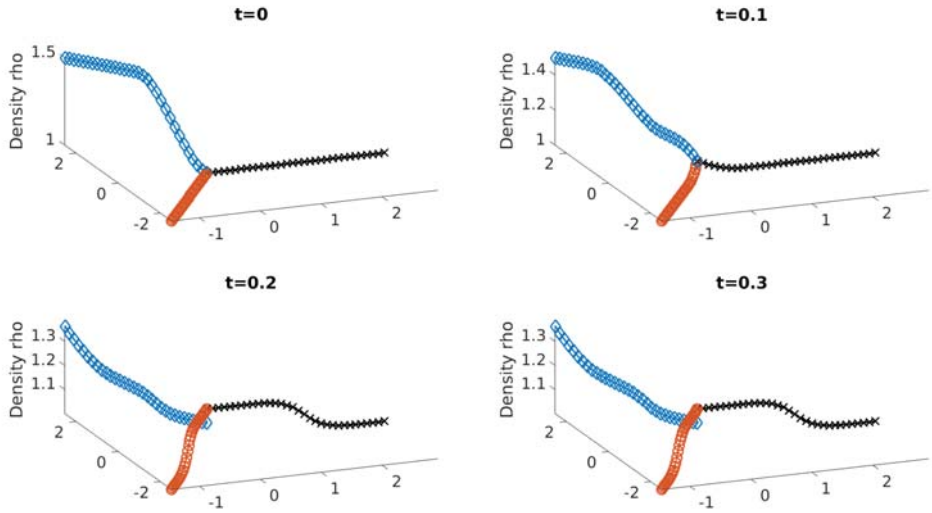

FIGURE 3. Evolution of Density ρ. Arcs: $\diamond$ $j = 1$, $\circ$ $j = 2$, $\times$ $j = 3$.

The Table 5.3 contains the L^1 errors and convergence rate of the coupled solution compared to a numerical solution of higher discretization at each arc ($j = 1, 2, 3$). The errors and order are computed analogously to table 5.2. Since the initial data in arc $j = 2$ and $j = 3$ are identical and the coupling handles all arcs the same way we get coniciding data for those both arcs. hence, we compress both data sets to one in the convergence tabel.

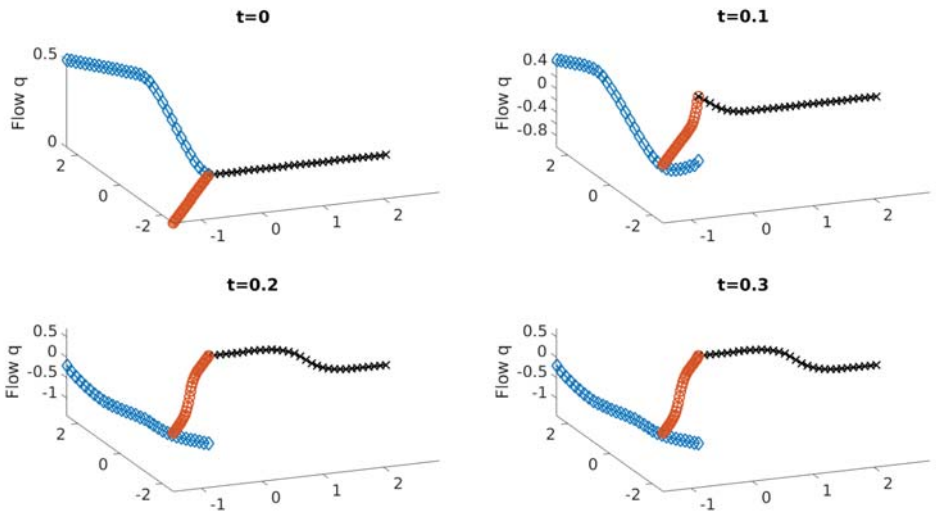

FIGURE 4. Evolution of Flow q. Arcs: $\diamond$ $j=1$, $\circ$ $j=2$, $\times$ $j=3$.

$j=1:\ N_k$	$L^1\ \rho$	$L^1\ q$	Rate ρ	Rate q
2^5	-7.6683	-5.6102	/	/
2^6	-9.2223	-7.1885	1.5541	1.5783
2^7	-10.7893	-8.7746	1.5669	1.5861
2^8	-12.3244	-10.3241	1.5351	1.5494
2^9	-13.7622	-11.7769	1.4378	1.4529
2^{10}	-15.1328	-13.1563	1.3706	1.3794
2^{11}	-16.5236	-14.5467	1.3908	1.3904
2^{12}	-18.1942	-16.2137	1.6706	1.6671
$j=2,3:\ N_k$	$L^1\ \rho$	$L^1\ q$	Rate ρ	Rate q
2^5	-8.8909	-6.5146	/	/
2^6	-10.5499	-8.1738	1.6591	1.6593
2^7	-12.4446	-10.0709	1.8947	1.8970
2^8	-14.3670	-11.9932	1.9223	1.9223
2^9	-16.3003	-13.9261	1.9333	1.9329
2^{10}	-18.2503	-15.8749	1.9500	1.9488
2^{11}	-20.2580	-17.8813	2.0077	2.0064
2^{12}	-22.4155	-20.0355	2.1575	2.1542

TABLE 4. L^1 convergence on a network with 3 arcs

Acknowledgements. This work has been partly supported by DFG excellence initiative and the excellence cluster EXC128, BMBF KinOpt and DAAD 55866082. This work is also based on the research supported in part by the National Research Foundation of

South Africa (Grant Number: 93476) and the Research Development Programme of the University of Pretoria.

References

[1] M. K. Banda, M. Herty, and A. Klar, *Coupling conditions for gas networks governed by the isothermal Euler equations*, Netw. Heterog. Media, 1 (2006), pp. 295–314 (electronic).

[2] ———, *Gas flow in pipeline networks*, Netw. Heterog. Media, 1 (2006), pp. 41–56.

[3] G. Bastin, J. Coron, and B. dAndréa Novel, *Using hyperbolic systems of balance laws for modeling, control and stability analysis of physical networks*, in Lecture notes for the Pre-congress workshop on complex embedded and networked control systems, 17th IFAC World Congress, 2008.

[4] G. Bastin, J. Coron, and B. dAndréa Novel, *On lyapunov stability of linearised saint-venant equations for a sloping channel*, Networks Heterogeneous Media, 4 (2009), pp. 177–187.

[5] R. Borsche and J. Kall, *Ader schemes and high order coupling on networks of hyperbolic conservation laws*, Journal of Computational Physics, 273 (2014), pp. 658–670.

[6] G. Bretti, R. Natalini, and B. Piccoli, *Fast algorithms for the approximation of a traffic flow model on networks.*, Discrete Contin. Dyn. Syst., Ser. B, 6 (2006), pp. 427–448.

[7] ———, *Fast algorithms for the approximation of a traffic flow model on networks*, Discrete Contin. Dyn. Syst. Ser. B, 6 (2006), pp. 427–448 (electronic).

[8] G. Bretti, R. Natalini, and B. Piccoli, *Numerical approximations of a traffic flow model on networks*, Netw. Heterog. Media, 1 (2006), pp. 57–84.

[9] J. Brouwer, I. Gasser, and M. Herty, *Gas pipeline models revisited: model hierarchies, nonisothermal models, and simulations of networks*, Multiscale Model. Simul., 9 (2011), pp. 601–623.

[10] R. Colombo and M. Garavello, *A well posed riemann problem for the p-system at a junction*, Netw. Heterog. Media, 1 (2006), pp. 495–511.

[11] R. M. Colombo and M. Garavello, *On the p-system at a junction*, in Control methods in PDE-dynamical systems, vol. 426 of Contemp. Math., Amer. Math. Soc., Providence, RI, 2007, pp. 193–217.

[12] ———, *On the Cauchy problem for the p-system at a junction*, SIAM J. Math. Anal., 39 (2008), pp. 1456–1471.

[13] R. M. Colombo, G. Guerra, M. Herty, and V. Schleper, *Optimal control in networks of pipes and canals*, SIAM J. Control Optim., 48 (2009), pp. 2032–2050.

[14] R. M. Colombo, M. Herty, and V. Sachers, *On* 2×2 *conservation laws at a junction*, SIAM J. Math. Anal., 40 (2008), pp. 605–622.

[15] R. M. Colombo and F. Marcellini, *Coupling conditions for the* 3×3 *Euler system*, Netw. Heterog. Media, 5 (2010), pp. 675–690.

[16] R. M. Colombo and C. Mauri, *Euler system at a junction*, Journal of Hyperbolic Differential Equations, 5 (2007), pp. 547–568.

[17] R. Courant, K. O. Friedrichs, and H. Lewy, *Über die partiellen differenzengleichungen der mathematischen physik*, Mathematische Annalen, 100 (1928), pp. 32–74.

[18] C. M. Dafermos, *Hyperbolic conservation laws in continuum physics*, vol. 325 of Grundlehren der Mathematischen Wissenschaften [Fundamental Principles of Mathematical Sciences], Springer-Verlag, Berlin, second ed., 2005.

[19] C. D'Apice, S. Göttlich, M. Herty, and B. Piccoli, *Modeling, simulation, and optimization of supply chains*, Society for Industrial and Applied Mathematics (SIAM), Philadelphia, PA, 2010. A continuous approach.

[20] C. D'Apice, R. Manzo, and B. Piccoli, *A fluid dynamic model for telecommunication networks with sources and destinations*, SIAM J. Appl. Math., 68 (2008), pp. 981–1003.

[21] C. D'Apice, R. Manzo, and B. Piccoli, *Existence of solutions to Cauchy problems for a mixed continuum-discrete model for supply chains and networks*, J. Math. Anal. Appl., 362 (2010), pp. 374–386.

[22] M. Garavello and B. Piccoli, *Traffic flow on a road network using the Aw-Rascle model*, Comm. Partial Differential Equations, 31 (2006), pp. 243–275.

[23] ———, *Traffic flow on networks*, vol. 1 of AIMS Series on Applied Mathematics, American Institute of Mathematical Sciences (AIMS), Springfield, MO, 2006. Conservation laws models.
[24] E. Godlewski and P.-A. Raviart, *Hyperbolic Systems of Conservation Laws*, Mathematiques and Applications, Ellipses, first ed., 1991.
[25] S. K. Godunov, *A difference scheme for the numerical computation of a discontinuous solution of the hydrodynamic equation*, Math. Sbornik, 47 (1959), pp. 271–306.
[26] M. Gugat, *Optimal nodal control of networked hyperbolic systems: evaluation of derivatives*, Adv. Model. Optim., 7 (2005), pp. 9–37 (electronic).
[27] B. Haut and G. Bastin, *A second order model of road junctions in fluid models of traffic networks.*, Netw. Heterog. Media, 2 (2007), pp. 227–253.
[28] M. Herty, C. Jörres, and B. Piccoli, *Existence of solution to supply chain models based on partial differential equation with discontinuous flux function*, J. Math. Anal. Appl., 401 (2013), pp. 510–517.
[29] M. Herty and M. Rascle, *Coupling conditions for a class of second-order models for traffic flow*, SIAM J. Math. Anal., 38 (2006), pp. 595–616.
[30] S. Jin and Z. P. Xin, *The relaxation schemes for systems of conservation laws in arbitrary space dimensions*, Comm. Pure Appl. Math., 48 (1995), pp. 235–276.
[31] O. Kolb, J. Lang, and P. Bales, *An implicit box scheme for subsonic compressible flow with dissipative source term*, Numer. Algorithms, 53 (2010), pp. 293–307.
[32] D. Kröner, *Numerical schemes for conservation laws*, Wiley Teubner, 1997.
[33] G. Leugering and J. Schmidt, *On the modelling and stabilization of flows in networks of open canals*, SIAM journal on control and optimization, 41 (2002), p. 164.
[34] R. J. LeVeque, *Finite volume methods for hyperbolic problems*, Cambridge Texts in Applied Mathematics, Cambridge University Press, 2002.
[35] H. Nessyahu and E. Tadmor, *Nonoscillatory central differencing for hyperbolic conservation laws*, J. Comput. Phys., 87 (1990), pp. 408–463.
[36] P. Sweby, *High resolution schemes using flux limiters for hyperbolic conservation laws*, SIAM Journal on Numerical Analysis, (1984), pp. 995–1011.
[37] S. Tan and C.-W. Shu, *Inverse Lax-Wendroff procedure for numerical boundary conditions of conservation laws*, J. Comput. Phys., 229 (2010), pp. 8144–8166.
[38] ———, *Inverse Lax-Wendroff procedure for numerical boundary conditions of hyperbolic equations: survey and new developments*, in Advances in applied mathematics, modeling, and computational science, vol. 66 of Fields Inst. Commun., Springer, New York, 2013, pp. 41–63.
[39] S. Tan, C. Wang, C.-W. Shu, and J. Ning, *Efficient implementation of high order inverse Lax-Wendroff boundary treatment for conservation laws*, J. Comput. Phys., 231 (2012), pp. 2510–2527.
[40] E. F. Toro, *Riemann Solvers and Numerical Methods for Fluid Dynamics: A Practical Introduction*, Springer, second ed., 2009.
[41] B. van Leer, *Towards the ultimate conservative difference scheme. v. a second-order sequel to godunov's method*, J. Comput. Phys., 32 (1979), pp. 101–136.